Morphology and size of the particles emitted from a gasoline direct injection-engine vehicle and their ageing in an environmental chamber

Jiaoping Xing[a,b], Longyi Shao[a] *, Wenbin Zhang[c], Jianfei Peng[d], Wenhua Wang[a], Shijin Shuai[c], Min Hu[d], Daizhou Zhang[e] *

[a]State Key Laboratory of Coal Resources and Safe Mining, School of Geoscience and Survey Engineering, China University of Mining and Technology (Beijing), Beijing 100083, China.

[b]2011 Collaborative Innovation Center of Jiangxi Typical Trees Cultivation and Utilization, School of Forestry, Jiangxi Agricultural University, Nanchang, 330045, China.

[c]State Key Laboratory of Automotive Safety and Energy, Department of Automotive Engineering, Tsinghua University, Beijing 100084, China

[d]State Key Joint Laboratory of Environmental Simulation and Pollution Control, College of Environmental Sciences and Engineering, Peking University, Beijing 100871, China

[e]Faculty of Environmental and Symbiotic Sciences, Prefectural University of Kumamoto, Kumamoto 862-8502, Japan

* Corresponding Author - e-mail: shaoL@cumtb.edu.cn (Longyi Shao); dzzhang@pu-kumamoto.ac.jp (Daizhou Zhang)

Highlights

1. GDI-engine vehicles emitted a large amount of both primary and secondary organic aerosols.
2. Higher contents of organic particles were emitted under hot stabilized running and hot start states.
3. Sulfate and secondary organic aerosol formed on the surface of primary particles after ageing.
4. Particles aged rapidly by catalyzed acidification under high pollution levels in Beijing.

Abstract:

Air pollution is particularly severe in developing megacities, such as Beijing, where vehicles equipped with modern gasoline direct injection (GDI) engines are becoming one of major sources of the pollution. This study presents the characteristics of individual particles emitted by a GDI gasoline vehicle and their ageing in a smog chamber under the Beijing urban environment, as part of the Atmospheric Pollution & Human Health (APHH) research programme. Using transmission electron microscopy, we identified the particles emitted from a commercial GDI-engine vehicle running under various conditions, namely, cold start, hot start, hot stabilized running, idle, and acceleration states. Our results showed that most of the particles were organic, soot and Ca-rich ones, with small quantities of S-rich and metal-containing particles. In terms of particle size, the particles exhibited a bimodal distribution in number *vs* size, with one mode at 800–900 nm, and the other at 140–240 nm. The amounts of organic particles emitted under hot start and hot stabilized states were higher than those emitted under other conditions. The amount of soot particles was higher under cold start and acceleration states. Under the idle state, the proportion of Ca-rich particles was highest, although their absolute number was low. In addition to quantifying the types of particles emitted by the engine, we studied the ageing of the particles during 3.5 hours of photochemical oxidation in an environmental chamber under the Beijing urban environment. Ageing transformed soot particles into core-shell structures, coated by secondary organic species, while the content of sulfur in Ca-rich and organic particles increased. Overall, the majority of particles from GDI-engine vehicles were organic

and soot particles with submicron or nanometric size. The particles were highly reactive; they reacted in the atmosphere and changed their morphology and composition within hours via catalyzed acidification that involved gaseous pollutants at high pollution levels in Beijing.

1. Introduction

Air pollution caused by $PM_{2.5}$ in megacities such as Beijing, the capital city of China, is of public and academic concerns due to its environmental impacts (Bond et al., 2013; Huang et al., 2014; Liu et al., 2017) and adverse health effects (Chart-asa and Gibson, 2015; Shao et al., 2017). Motor vehicle emissions are one of the most significant sources of airborne particles in the urban atmosphere (Hwa and Yu, 2014), and contribute up to 31% of primary particulate emissions of $PM_{2.5}$ in Beijing (Yu et al., 2013). Moreover, secondary aerosol formation associated with traffic emissions is a major process leading to the rapid increase of $PM_{2.5}$, which results in severe haze episodes (Huang et al., 2014). Although emissions from gasoline engines are relatively lower than those from diesel engines (Alves et al., 2015), the number of gasoline-powered vehicles in urban areas greatly exceeds that of diesel-powered vehicles. The total number of vehicles in China reached 310 million in 2017, about 70% of these were powered by gasoline engines (National Bureau of Statistics of China, 2018). There are two main types of gasoline engines, namely, conventional multipoint port fuel injection (PFI) engines and gasoline direct injection (GDI) engines. In recent years, the demand for engines with high efficiency and low fuel consumption has led to an increasing use

of GDI engines in light-duty passenger cars. The market share of GDI-engine vehicles has increased dramatically over the past decade and was estimated to reach 50% of new gasoline vehicles sold in 2016 (Zimmerman et al., 2016). In Beijing and northern China, the vehicle emissions become a more concerning issue in terms of air pollution when the emission from coal combustion are seriously reduced after the Action for Comprehensive Control of Air Pollution in Beijing since 2017 (Chang et al., 2019; Chen et al. 2019; Zhang et al. 2019). In spite of this, regional transport of coal-burning emissions from the surrounding areas can still influence the urban air sometimes severely in winter (Ma et al., 2017; Zhang et al., 2019).

The number, mass and size distribution of particles emitted from GDI-engine vehicles have been studied (Khalek et al., 2010; Maricq et al., 2011; Baral et al., 2011). The size distribution usually has an accumulation mode with the maxima in the diameter range of 100–300 nm. Major components of the particles include elemental carbon (EC), organic carbon, and ash (Giechaskiel et al., 2014). Besides particulate matter, the engines emit gaseous hydrocarbon compounds. These compounds might form particles, or be adsorbed on the surface of particle aggregates, leading to the growth of the particles in the engine emission (Luo et al., 2015). Relatively high particle emissions by GDI-engine vehicles have prompted studies on the effects of engine operating parameters and fuel composition on the characteristics of the particles (Hedge et al., 2011; Szybist et al., 2011). It has been found that, in general, emissions under the cold start condition make up the major contribution to the total amount of PM emissions from GDI engines (Chen and Stone, 2011). Studies have also demonstrated that the

highest particle emissions from GDI engines in number concentration occur under the acceleration state during transient vehicle operations (Chen et al., 2017).

Studies have also shown that gasoline vehicles are an important source of secondary aerosol precursors in urban areas (Suarez-Bertoa et al., 2015). Secondary aerosols can be formed via gas-phase reactions of volatile organic compounds and multiphase and heterogeneous processes of primary particles (Zhu et al., 2017). Experiments performed in environmental chambers demonstrated that the mass of secondary aerosols derived from precursors could exceed that of directly-emitted aerosols (Jathar et al., 2014). The occurrence of secondary aerosols on particles could change the properties of particles in size, mass, chemical composition, morphology, optical and hygroscopic parameters. These changes, in turn, might affect the environmental impact of the particles significantly, for instance in terms of visibility, human health, weather, and energy budgets (Laskin et al., 2015; Peng et al., 2017). In general, the ageing processes of primary particles in the atmosphere are studied to understand their climate effects (Niu et al., 2011). However, the lack of data on primary particles emitted by gasoline engines hinders a deep understanding of the roles and activities of the particles in ambient air pollution and relevant environmental effects.

Atmospheric Pollution & Human Health (APHH) research programme aimed to explore the sources and processes affecting urban atmospheric pollution in Beijing. Details regarding this project are given in Shi et al. (2018). To address one of the aims of the AIRPOLL-Beijing (Source and Emissions of Air Pollutants) and AIRPRO-Beijing (The integrated Study of AIR Pollution Processes), we employed a dedicated

experiment to investigate the characteristics of the individual particles, in terms of the number concentration, size distribution, emitted from a GDI-engine vehicle during a real-world driving cycle for chassis dynamometer test, i.e., the Beijing driving cycle (BDC). Various test modes were introduced to accurately evaluate the emission from light- or medium-duty vehicles. Furthermore, experiments were conducted in an environmental chamber to investigate the ageing processes of particles emitted by GDI-engine vehicles in ambient air in Beijing. We utilized a transmission electron microscope equipped with an Oxford energy-dispersive X-ray spectrometer (TEM-EDX) to identify the morphology, size and elemental composition of particles emitted by the GDI-engine vehicle when it was running under different states. Particles before and after a 3.5-hour ageing in the chamber were compared on the basis of the TEM-EDX analysis. The TEM-EDX analysis provides the information on the internal inhomogeneity, mixing state and surface characteristics of individual particles and has been used to analyze the aerosol particles (Li and Shao, 2009; Loh et al., 2012; Adachi and Buseck, 2015; Shao et al., 2017). The experimental design allows for the study of the physical and chemical characteristics of the particles emitted from the GDI-engine vehicles, as well as their ageing in a simulated urban atmosphere. The purposes of this study are to evaluate the individual characteristics and the ageing process of primary particles emitted by a GDI-engine vehicle, to investigate the ageing processes of such particles in the atmosphere, and to deepen the understanding of the environmental impact of gasoline-powered vehicle emissions.

2. Material and methods

2.1 Test vehicle, fuels, and test procedure

The GDI-engine vehicle utilized in the experiment complies with the China Phase 4 (equivalent to Euro 4) standard. It uses a three-way catalyst to reduce gaseous emissions. The GDI (model GDI-1.4-T) in the test vehicle is recognized as a representative of leading-edge designs of gasoline engines, because of its advanced engine technologies such as its better fuel burning efficiency and lower greenhouse gas emissions than other types of engine. Vehicles equipped with such GDI engines constitute the majority of light-duty vehicles in China, especially in large cities like Beijing. Details of the engine used in this study are listed in Table S1. The fuel used in the experiment is a commercial gasoline blend of common quality in China. The properties of the fuel were measured by SGS-CSTC Standards Technical Services Co., Ltd., China, and are listed in Table S2. The fuel has a Research Octane Number (RON) of 93 and is a fifth-stage gasoline. It contains 36.7% of aromatics and 15.4% of olefins in volume and has 6% of sulfur in mass, representing a typical fifth-stage gasoline in China (with high aromatics) and is now widely used in Beijing. The experiments were conducted within repeated Beijing Driving Cycles (BDCs), and one BCD included a 200-s “cold start” phase followed by an 867-s “hot stabilized running” phase. The conditions during a BDC in the experiments are illustrated in Figure S1a. The cold start state was achieved by starting the vehicle with a period of small accelerations, while the hot stabilized running state had multiple periods of large acceleration and a maximum velocity of 50 km h^{-1}. The BDC, characterized by a higher proportion of idling periods and a lower acceleration speed than the New European Driving Cycle

(NEDC), was performed to simulate the repeated braking and acceleration on road in megacities such as Beijing.

All tests were performed on a Euro 5/LEV2/Tier 2-capable test cell on a 48-inch single-roll chassis dynamometer at the State Key Laboratory of Automobile Safety and Energy Conservation at Tsinghua University. The test procedure for each run was as follows: fuel change, BDC preparation, soak, cold start BDC test, and hot start BDC test. After fuel change and BDC preparation, the test vehicle was then conditioned with an overnight soak for more than 10 h. The soak room temperature was maintained between 20 and 30 °C. Due to the limitation of the facilities and available running time, a hot start test was conducted within 5 mins after the cold start test. A dilution unit was applied to dilute the exhaust from the tailpipe into 1/10 in volume using synthetic air composed of 79% N_2 and 20% O_2, in order to obtain the concentrations suitable for subsequent measurements and suppress possible coagulation. The number concentration of the emitted particles was monitored by a Combustion Fast Particle Size Spectrometer Differential Mobility Spectrometer 500 (DMS 500). The maximum measurable number concentration of DMS 500 was 10^{11} (dN/dlogDp/cc) after the dilution (Petzold et al., 2011). For the analyses of individual particles, 6–8 samples were collected during one BDC test. At least one sample was collected under each running state (i.e. cold start, hot start, idle state, acceleration state, or hot stabilized running state). The driving cycle test was repeated at least twice. Two or more samples were obtained for each running state. A single-stage cascade impactor (KB-2, Qingdao Jinshida Company) was mounted to the exit of the tailpipe after the dilution unit. The

emitted particles were collected onto 300-mesh copper TEM grids, which were covered with a carbon-coated formvar film. The flow rate was 1.0 L min^{-1}, and the cut-off diameter of the impactor for 50% collection efficiency was 0.25 μm if the density of the particles was 2 g cm^{-3}. For each sample, the collection time was 60 s.

2.2 Environmental chamber experiments

Particles from the GDI-engine vehicle were introduced into an environmental chamber and exposed to sunlight. The chamber, made of Teflon(tm) perfluoroalkoxy (PFA) polymer in order to achieve a high transmission of ultraviolet light, has an internal volume of 1.2 m^3. Ambient sunlight was used as the driving force for photochemical reactions in the chamber, in an environment close to actual open air. Before the experiments, the chamber was cleaned by flushing with zero air for approximately 12 hours and illuminated with sunlight, to remove residues that could influence the experiments. H_2O_2 (1 mL, 30%), together with the vehicle emission, was injected into the chamber to generate OH exposure. The OH exposure at the end of the experiments reproduced extreme oxidation processes, which were equivalent to cases of an oxidation more than 10 days in Beijing ambient air if the 24-hour-mean concentration of OH is 10^6 molecules cm^{-3} (Lu et al., 2013). The aging experiments for the gasoline exhausts were carried out with a relatively high OH exposure compared to ambient conditions in order to obtain the aging process. This method and the amount of H_2O_2 have been frequently used in smog chamber experiments (Song et al., 2007; Song et al., 2019). After the injection, the experiments were conducted from approximately 13:00 to 17:00 local time under sunshine, with the relative humidity being kept at around 50%. The global solar radiation when the tests were carried out

was approximately 318 W m^{-2}. After 3.5 h of ageing, the particles in the chamber were collected onto mesh TEM grids using the impactor. The collection time for each sample was 120 s. The schematic diagram of the experimental system is presented in Figure S1b.

2.3 TEM/EDX and scanning transmission electron microscopy (STEM) analyses

The particles in the samples were examined using a Tecnai G2 F30 field emission high-resolution transmission electron microscope (FE-HRTEM). This microscope is also equipped with an Oxford EDX and a STEM unit with a high-angle annular dark-field detector (HAADF). The EDX can detect elements with the atom number larger than 5 (B) in a single particle. The HAADF can detect the distribution of a certain element by mapping the distribution of the element in a particle. The TEM was operated with the acceleration voltage of 300 kV. EDX spectra were firstly collected for 20 live seconds to minimize the influence of radiation exposure and potential beam damage and then for 90 live seconds for a range of possible elements. Copper was excluded from the analysis because of interference from the TEM grids which were made of copper.

To ensure the representativeness of the analyzed particles, more than 150 particles from at least 3 random areas were analyzed from the center and periphery of the sampling spot on each grid. All individual particles larger than 50 nm in the selected areas were analyzed. The TEM images were digitized using an automated fringe image processing system named Microscopic Particle Size of Digital Image Analysis System (UK) to project the surface areas of the particles. The equivalent spherical diameter of

a particle was calculated from its projected area, expressed as the square root of 4 A/π, where A was the projected area. The electron microscope analysis of individual particles was very time consuming, which hindered us from analyzing more particles from multiple engines emission. There are differences in emissions from vehicles to vehicles, even for vehicles with same model engines. Only one GDI vehicle, the type of which constitutes the majority of light-duty vehicles in China, was tested in this study. The representativeness of the present results remains unevaluated carefully with, such as, comparisons between vehicles to achieve broader statistical results, although the tests in the present studies were conducted under strict control conditions.

3. Results

3.1. Particle morphology, elemental composition and size

A total of 2880 particles were analyzed from the GDI-engine vehicles. Most of the particles were in the sub-micrometer size range. Based on morphology and elemental composition of the particles, the majority of them were identified as soot, organic and Ca-rich particles, a smaller amount was identified as S-rich or metal-rich particles (Fig. 1). The method of particle classification is similar to that adopted by Okada et al. (2005) and Xing et al. (2019). In the following description, "X-rich" means that the element "X" occupies the largest proportion in the element composition of the particles. Figure 2 illustrates the number-size distributions of the relative concentration (dN/dlogD) of primary particles from the GDI-engine vehicle, where N is the relative number fraction and D is the equivalent diameter. The particles were in the range of 60–2500 nm and displayed a bimodal distribution, with one mode in the 140–240 nm range, and another in the 800–900 nm range. Particles smaller than 250 nm were largely underestimated

because of the loss during the particle collection. Therefore, there should have been more particles in the smaller mode range than shown in Figure 2. Concerning the loss of small particles, we measured the size distribution by the DMS500 (Fig. S2). The results showed that a large amount of nucleation mode particles were emitted by the GDI vehicle.

It should be noted that organic particles were mainly composed of C and O elements, and contained a small amount of inorganic elements Ca, P, S and Zn. Elemental mapping of the organic particles exhibited the presence of Ca, P, S and Zn in some of the particles, showing the mixture state of organic and inorganic materials (Fig. 1f). It has been reported that such particles could be related to the combustion of fuels or lubrication oil (Rönkkö et al., 2013). In addition to these primary organic particles, the GDI-engine vehicle emitted precursor gases, which produced secondary organic particles via gas-phase reactions, and multiphase and heterogeneous processes on the primary particles. A group of spherical particles were found in the environmental chamber (Fig. 1g). These particles became semi-transparent or transparent to an electron beam, which was characteristic of organic materials, liquid water, or their evaporation residues either mixed or not mixed with electron absorptive materials. We regarded these particles as secondary organic particles because the humidity in the chamber during the experiment was kept much below saturation (relative humidity around 50%). Therefore, these particles were expected to mainly consist of secondary organic materials, which should have been produced via gas phase reactions or on the surface of pre-existing particles (Hu et al., 2016). No other elements, except C and O,

were identified in these particles, which was consistent with the above inference. Similar particles were also encountered in other environmental chamber experiments studying emissions from light-duty gasoline vehicles (Jathar et al., 2014).

3.2 Number fractions of particles

Figure 3 illustrates the numbers of accumulation mode particles emitted by burning one kilogram of fuel during the cold start and hot start driving cycles. PM emissions at the start-up stage under both cold and hot start states were higher than the emissions under the states when the engine was fully warmed and the vehicle operation was stabilized. The PM emission was the highest under the hot stabilized running state (2.3×10^{10} particles (kg fuel)$^{-1}$), followed by those under the hot start (1.2×10^{10} particles (kg fuel)$^{-1}$), cold start (7.1×10^{9} particles (kg fuel)$^{-1}$), and acceleration running states (2.9×10^{9} particles (kg fuel)$^{-1}$), with the emission under the idle running state being the lowest (7.4×10^{8} particles (kg fuel)$^{-1}$) (Fig. S3). The higher emission of particle in terms of number for the GDI vehicle under the hot start state can be ascribed to the experimental time of the vehicle engine. The hot start test in this study was conducted within 5 mins after the cold start test. The PM emissions from GDI vehicles were relatively less affected by ambient temperature for the initial 30 minutes during the warming up of the engines (Cotte et al., 2001). This may lead to the high value of the PM emission for the hot start state which is slightly higher than that for the cold start state. Although the total PM emission were higher under hot start state than that under the cold start state, the comparison of those in the size range of accumulation mode indicates that the particulate emissions for this mode of particles were higher under the

303 cold start state than under the hot start sate (Fig. 3). This can be attributed to the less
304 efficiency of the vaporization of fuel droplets in the combustion cylinder under the cold
305 start state (Chen et al., 2017). Size distributions of the particles varied with driving
306 conditions (Fig. S4). Under the cold start state and acceleration running state, higher
307 number concentrations, and thus higher mass concentrations of the particles with
308 accumulation mode were emitted in comparison with other running states.

309 Under all the running states, morphologies and types of the particles remained
310 similar but the proportions of different types of particles differed considerably (Fig. S5).
311 The proportion of organic particles was high under hot stabilized and hot start states.
312 Soot particles were abundant under cold start and acceleration states. A relatively higher
313 proportion of Ca-rich particles was found under idle state, compared to those under
314 other running states.

315 We estimated the number of different type particles in the emission under the
316 running states by burning one kilogram of fuel (Fig. 4). Organic particles in the
317 emission under the hot stabilized running state (2.3×10^{9} particles (kg fuel)$^{-1}$) and the
318 hot start running state (3.6×10^{8} particles (kg fuel)$^{-1}$) were higher than in the emission
319 under other running states. The number of soot particles were higher under the hot
320 stabilized running state (1.7×10^{9} particles (kg fuel)$^{-1}$) and the cold start state (5.9×10^{8}
321 particles (kg fuel)$^{-1}$) than those under other running states. Under the idle state, the
322 relative proportion of Ca-rich particles was the highest, although their absolute number
323 was low (1.4×10^{9} particles (kg fuel)$^{-1}$).

324 Under the cold start state, a significant proportion of the emitted particles were

soot particles. This can be attributed to the incomplete vaporization of fuel droplets in the combustion cylinder (Chen et al., 2017). Under the hot start state and the hot stabilized running state, organic particles were predominant. Under these two running states, the engine temperature was high, which enabled the fuel to evaporate and mix with the air easily. With the increase of the temperature in the cylinders, the rate of particle oxidation increased, which could cause an increase of organic particles in the emission (Fu et al., 2014). Under the idle state, the fuel consumption was much lower than that under the other running states, which resulted in a higher relative contribution to particles from lubricant oil. The high Ca content in the lubricant oil led to a higher Ca-rich particle emission under this running state. Under the acceleration state, the predominant types of particle included soot, organic, and Ca-rich particles. As the acceleration running required a high vehicular speed and engine load, the emissions contained more soot particles than those under other running states.

3.3. Aged particles in the environmental chamber

A large amount of secondary organic particles (accounting for 80%-85% in number), some soot particles, Ca-rich particles, and primary organic particles were detected in the environmental chamber (Fig. 5). After the ageing process, many soot particles changed into core-shell structures and became coated with secondary species (Figs. 5b and 5c). The EDX results showed that almost all coatings were mainly composed of C, O, and S, suggesting these coatings were a mixture of organic and sulfate. The morphology and compositions of Ca-rich particles and organic particles (Figs. 5e and 5g) changed, with the aged ones having a more irregular shape and a higher sulfur content in comparison with fresh ones (Figs. 5A and B).

Approximately 80% of the soot particles were present in core-shell structures and coated with secondary species after the 3.5-hour ageing. In contrast, before the ageing, the particles with a core-shell structure were only about 10% of the total. The mean diameter of the soot particles after ageing was around 0.49 μm, which was much smaller than that before the ageing (0.65 μm), indicating the shrinkage of the soot particles during the ageing (Fig. 5b). The core-shell ratios, defined as the ratio of the diameter of the core part (Dcore) to the diameter of the whole particle (Dshell) (Niu et al., 2016; Hou et al., 2018), were used to quantify the aging degree of the soot particles with coating. It was found that the core-shell ratios of the soot particles in the smog chamber were mainly in the range of 0.25–0.78, indicating the stronger aging degree of soot particles in the chamber than case data in urban air with the ratios of 0.4–0.9 (Niu et al., 2016)."

4. Discussion

4.1. Contribution of GDI-engine vehicle emissions to urban air pollution

Our investigation showed that the GDI-engine vehicle emitted a large amount of organic particles (32%), soot (32%), Ca-rich particles (26%), S-rich (5%) and metal-containing particles (4%). Relevant studies have also shown that the primary carbonaceous aerosols (element carbon + primary organic aerosol) accounted for 85 % of the PM in the GDI vehicles, suggesting that carbonaceous aerosols were the major contributors in the PM from GDI gasoline vehicles (Du et al., 2018). Considering the large fraction of the vehicles equipped with GDI engines in megacities like Beijing, this indicates a possible substantial contribution of GDI-engine vehicles to urban air

370 pollution. Moreover, organic particles occupied the majority of the particles emitted
371 under hot stabilized running and hot start states. It has been noted that the organic matter
372 was the major component of the total particle mass during the hot start conditions
373 (Fushimi et al., 2016; Chen et al., 2017), which was consistent with the results obtained
374 for the number concentrations in our study. The hot stabilized running state is the most
375 frequent running condition of vehicles, whereas the hot start state is the most frequent
376 condition in congested traffic. This suggests that a substantial number of organic
377 compounds in the air pollution of populated cities might be directly related to vehicle
378 emissions.

379 Organic particles and soot particles in ambient air are emitted from a range of
380 sources including fossil fuels, biomass burning and urban waste burning (Kanakidou et
381 al., 2005). Table 1 shows the major characteristics of particles in the emissions from
382 different sources. For instance, there is a higher fraction of soot particles and a lower
383 fraction of organic particles in the emissions of GDI-engine vehicles compared to PFI-
384 engine vehicles (Xing et al., 2017). Organic particles in emissions from gasoline
385 vehicles are usually enriched in Ca, S and P (Xing et al., 2017; Liati et al., 2018). In
386 comparison, emissions from biomass/wood burning are usually dominated by organic
387 particles, which account for more than 50% of the total amount of particles (Liu et al.,
388 2017). Furthermore, organic particles from biomass/wood burning usually show
389 elevated K content, and thus, this element is frequently used as an indicator for
390 biomass/wood burning organic particles (Niu et al., 2016). Observations of primary
391 particles directly from coal burning have also demonstrated a predominance of organic

particles, soot particles, S-rich particles and mineral particles (Zhang et al., 2018; Wang et al., 2019). Both biomass burning and coal combustion can produce organic particles and almost all the emitted particles contain a certain amount of Si in addition to C and O. Table 1 also shows the elemental concentrations in the organic particles in the emissions from different types of sources. Since the concentrations of minor elements in the organic particles are highly dependent on the sources, they could be used for source identification of individual particles in the atmosphere.

The present data also permit the compilation of a rough inventory of particle categories and amounts emitted from GDI-engine vehicles under various running conditions (Fig. 4). Combined with statistics on the number of vehicles with GDI engines, the running time and the running conditions on roads within a certain area, it is possible to make an approximate estimate of the amounts of primary particles emitted from GDI-engine vehicles. Such estimate is the basis for accurate source apportionment of particles from vehicles, and it will be very beneficial for studies on the anthropogenic sources of primary particles in urban air. These data could be brought together to better understand the sources of air pollutants in the Beijing megacity and to improve the capability of developing cost-effective mitigation measures.

4.2 Rapid ageing of primary particles in Beijing

The results of chamber experiments indicate that sulfate and secondary organic aerosol (SOA) form on the surface of soot, Ca-rich and organic particles. Moreover, the atmospheric transformation of primary particles emitted by the GDI-engine vehicles could occur within 3.5 hours, indicating the ageing was rapid. Peng et al. (2014) found

414 similar timescales for black carbon transformation under polluted conditions in Beijing.
415 The rapid ageing of primary particles could be caused by several factors, such as the
416 concentration of gaseous pollutants from the vehicles, strength of solar radiation,
417 relative humidity (RH), and O_3 concentration (Guo et al., 2012; Deng et al., 2017; Du
418 et al., 2018). The present experiments were conducted in the atmosphere with relative
419 humidity of approximately 50% and solar radiation of 318 Wm^{-2}. The total hydrocarbon
420 emission (THC) from the GDI vehicles was 0.297 g km^{-1}. Repeated braking and
421 acceleration in the BDC could cause incomplete combustion and consequently high
422 THC emission. Under a high concentration of gaseous pollutants, primary particles
423 would age rapidly when exposed to solar radiation. Consequently, secondary species
424 including SOA and sulfate were produced on or condensed onto the particles, leading
425 to the coating. Guo et al. (2014) also showed that secondary photochemical growth of
426 fine aerosols during the initial stage of haze development could be attributed to highly
427 elevated levels of gaseous pollutants.

428 The mixture of SOA and sulfate have been detected in our chamber experiment,
429 indicating the involvement of inorganic salts in the SOA formation. Previous studies
430 have demonstrated the enhancement of SOA production in the presence of inorganic
431 sulfate (Beardsley and Jang, 2015; Kuwata et al., 2015), and this is because sulfate can
432 catalyze carbonyl heterogeneous reactions, and consequently, lead to SOA production
433 (Jang et al., 2002; Jang et al., 2004). Moreover, these aged primary particles favored
434 the formation of secondary aerosols by providing reaction sites and reaction catalysts.
435 Sulfate and secondary organic aerosol (SOA) co-existed on the surface of primary

particles, such as soot, Ca-rich and organic particles. In addition, the products of VOCs oxidation could react with SO_2 to rapidly produce sulfate (Mauldin et al., 2012). Thus, the rapid ageing of primary particles could also be attributable to the acid-catalyzed mechanism. As the major source of pollutants in urban air, the GDI-engine vehicles supply both primary particles and precursor gaseous species, and the rapid ageing of the particles under certain conditions is very likely to be the major driving force for the elevation of urban air pollution.

4.3 Implications and perspectives

Our results indicated that GDI-engine vehicles emitted a large amount of both primary and secondary organic aerosols. PM number emission of organic particles from GDI-engine vehicle were 2.9×10^{9} particles $(\text{kg fuel})^{-1}$ during the BDC. Secondary organic particle was predominant in the secondary aerosols, accounting for 80-85%% particles in the chamber. Organic aerosols (OA) play an important role in the Earth's radiation balance not only for its absorption and scattering of solar radiation but also because they can alter the microphysical properties of clouds (Scott et al., 2014). Particle size, shape, mixing state and composition affect their light scatterings and absorption cross sections, and cloud condensation nuclei activity (Jacobson, 2001). OA are composed of various types of chemical compounds with varying absorption properties (mixing state), which are determined by the emission sources, the formation mechanism (Zhu et al., 2017), and the source regions (Laskin et al., 2015). Primary OA from biomass burning is co-emitted with soot (black carbon), inorganic salts, and fly ash, producing internally and externally mixed particles in which the organic

components are present in different relative abundance (Lack et al., 2012). Similarity, primary OA in the exhaust of gasoline and diesel vehicles are mixed with Ca, P, Mg, Zn, Fe, S, and minor Sn inorganic compounds (Liati et al., 2018). In addition, previous measurements have indicated that SOA usually exists as an internal mixture with other aerosols, such as sulfate, ammonium, or nitrate (Zhu et al., 2017). Our results showed that the POA emitted from GDI-engine vehicle were mixed with soot, inorganic components such as Ca, P, and Zn. Some of the SOA formed in the smog chamber were mixed with sulfate. The complexity of mixing state makes it difficult to characterize the properties of OA. Lang-Yona et al. (2010) have found that for aerosols consisting of a strongly absorbing core coated by a non-absorbing shell, the Mie theory prediction deviate from the measurements by up to 10%. Moreover, atmospheric aging process, involving aqueous-phase aging and atmospheric oxidation, can either enhance or reduce light absorption by OA (Bones et al., 2010). The condensation process may result in a dramatic enhancement of hydrolysis of OA compounds, affecting their absorption spectra (Lambe et al., 2015).

Our results also showed that primary organic aerosols (POA) emitted by GDI-engine vehicles could acquire OA and sulfate coatings rapidly, within a few hours, and increase a sizable fraction of total ambient aerosols existing as internal mixtures. In addition, the fast ageing further caused the increase of aged POA in the total OA, consequently, largely modified the properties of the particles such as their optical properties. The results of the experiments in the chamber showed that most of the aged POA had a core-shell structure, whereas most of the secondary organic aerosols (SOA)

produced by gas-phase reactions had a uniform structure. These results push forward the understanding on the mixing state and chemical composition of both POA and SOA. The experimental data will benefit the parameterization of vehicles emissions in numerical models dealing with urban air pollution.

5. Conclusions

1. Five types of individual particles emitted by a GDI-engine gasoline vehicle were identified, including soot, organic, Ca-rich, S-rich, and metal-rich particles. Among them, soot, organic, and Ca-rich particles were predominant. The particles emitted from this commercial GDI-engine gasoline vehicle displayed a bimodal size distribution.
2. The concentrations of the particles emitted by this commercial GDI-engine gasoline vehicle vary with different running conditions. The PM emission was the highest under the hot stabilized running state, followed by those under the hot start, cold start, and acceleration running states, with the emission under the idle running state being the lowest under the idle running state.
3. The relative proportions of the different types of particles emitted by this commercial GDI-engine gasoline vehicle varied with different running conditions. Large amounts of organic particles were emitted during hot stabilized and hot start states. Under cold start and acceleration states, the emissions were enriched in soot particles. Under idle state, a relatively higher number of Ca-rich particles was emitted, although the absolute number was low.
4. After ageing in the environmental chamber, the structure of the soot particles

changed into a core-shell structure, and the particles were coated with condensed secondary organic material. Ca-rich particles and organic particles also were modified, and their content of sulfur increased after ageing.

5. Ageing of the emitted particles occurred rapidly, within hours. Such rapid ageing could be attributable to an acid-catalyzed mechanism and to the high initial concentrations of gaseous pollutants emitted by this commercial GDI-engine gasoline vehicle.

Data availability

All data presented in this paper are available upon request. Please contact the corresponding author (shaoL@cumtb.edu.cn).

Author contribution

LS designed this study; JX performed the experiments. JX, LS, DZ summarized the data and wrote the paper. WZ, JP, WW, SS, MH supported the experiments and commented the paper.

Competing interests

The authors declare that they have no conflict of interest.

Acknowledgements

This work was supported by Projects of International Cooperation and Exchanges NSFC (Grant No. 41571130031). The data analysis was partly supported by Science and Technology Project Founded by the Education Department of Jiangxi Province (No. GJJ180226), The Open Foundation of Jiangxi Province Key Laboratory of the Causes

and Control of Atmospheric Pollution, East China University of Technology (No. AE1902), Yue Qi Scholar Fund of China University of Mining and Technology (Beijing), and a Grant-in-Aid for Scientific Research (B) (No.16H02942) from the JSPS.

References

Adachi, K., and Buseck, P. R.: Changes in shape and composition of sea-salt particles upon aging in an urban atmosphere, Atmos. Environ., 100, 1-9, http://dio.org/10.1016/j.atmosenv.2014.10.036, 2015.

Alves, C. A., Lopes, D. J., Calvo, A. I., Evtyugina, M., Rocha, S., and Nunes, T.: Emissions from light-duty diesel and gasoline in-use vehicles measured on chassis dynamometer test cycles, Aerosol Air Qual. Res., 15(1), 99-116, http://dio.org/10.4209/aaqr.2014.01.0006, 2015.

Baral, B., Raine, R., and Miskelly, G.: Effect of engine operating conditions on spark-ignition engine PAH emissions, SAE Technical Paper 2011-01-1161, http://dio.org/10.4271/2011-01-1161, 2011.

Beardsley, R.L., and Jang, M.: Simulating the SOA formation of isoprene from partitioning and aerosol phase reactions in the presence of inorganics, Atmos Chem Phys, 15, 33121-33159, http://dio.org/10.5194/acpd-15-33121-2015, 2015.

Bond, T. C., Doherty, S. J., Fahey, D. W., Forster, P. M., Berntsen, T., DeAngelo, B. J., Flanner, M. G., Ghan, S., Kärcher, B., Koch, D., Kinne, S., Kondo, Y., Quinn, P. K., Sarofim, M. C., Schultz, M. G., Schulz, M., Venkataraman, C., Zhang, H., Zhang, S., Bellouin, N., Guttikunda, S. K., Hopke, P. K., Jacobson, M. Z., Kaiser, J. W., Klimont, Z., Lohmann, U., Schwarz, J. P., Shindell, D., Storelvmo, T., Warren, S. G., and Zender, C. S.: Bounding the role of black carbon in the climate system: A scientific assessment, J. Geophys. Res.-Atmos., 118(11), 5380-5552, http://dio.org/10.1002/jgrd.50171, 2013.

Bones, D.L., Henricksen, D.K., Mang, S.A., Gonsior, M., Bateman, A.P., Nguyen, T.B., Cooper, W.J., and Nizkorodov, S.A.: Appearance of strong absorbers and fluorophores in limonene-O_3 secondary organic aerosol due to NH^{4+}-mediated chemical aging over long time scales, J Geophys Res, 115, http://dio.org/10.1029/2009JD012864, 2010.Chart-asa, C., and Gibson, J. M.: Health impact assessment of traffic-related air pollution at the urban project scale: Influence of variability and uncertainty, Sci. Total Environ., 506-507, 409-421, http://dio.org/10.1016/j.scitotenv.2014.11.020, 2015.

Chang, L., Shao, L., Yang, S., Li, J., Zhang, M., Feng, X., Li, Y., 2019, Study on variation characteristics of $PM_{2.5}$ mass concentrations in Beijing after the action for comprehensive control of air pollution. Journal of Mining Science and Technology, 2019, 4(6): 539-546. http://dio.org/10.19606/j.cnki.jmst.2019.06.009. (in Chinese with English Abstract)

Chart-asa, C., and Gibson, J. M.: Health impact assessment of traffic-related air pollution at the urban project scale: Influence of variability and uncertainty, Sci. Total Environ., 506-507, 409-421, http://dio.org/10.1016/j.scitotenv.2014.11.020, 2015.

Chen, Z., Chen, D., Xie, X., Cai, J., Zhuang, Y., Cheng, N., He, B., and Gao, B.: Spatial self-aggregation effects and national division of city-level $PM_{2.5}$ concentrations in China based on spatio-temporal clustering, J. Clean. Prod., 207, 875-881, http://dio.org/10.1016/j.jclepro.2018.10.080, 2019.

564 Chen, L., Liang, Z., Zhang, X., and Shuai, S.: Characterizing particulate matter emissions from GDI and
565 PFI vehicles under transient and cold start conditions, Fuel, 189, 131-140,
566 http://dio.org/10.1016/j.fuel.2016.10.055, 2017.
567 Chen, L., and Stone, R.: Measurement of enthalpies of vaporization of isooctane and ethanol blends and
568 their effects on PM emissions from a GDI engine, Energ. Fuel, 25(3), 1254-1259,
569 http://dio.org/10.1021/ef1015796, 2011.
570 Cotte, H., Bessagnet, B., Blondeau, C., Mallet-Hubert, P.Y., Momique, J.C., Walter, C., Boulanger, L.,
571 Deleger, D., Jouvenot, G., Pain, C., and Rouveirolles, P.: Cold-start emissions from petrol and diesel
572 vehicles according to the emissions regulations (from Euro 92 to Euro 2000), Int J Vehicle Des, 27,
573 275-285, 10.1504/IJVD.2001.001971, 2001.
574 Deng, W., Hu, Q., Liu, T., Wang, X., Zhang, Y., Song, W., Sun, Y., Bi, X., Yu, J., Yang, W., Huang, X.,
575 Zhang, Z., Huang, Z., He, Q., Mellouki, A., and George, C.: Primary particulate emissions and
576 secondary organic aerosol (SOA) formation from idling diesel vehicle exhaust in China, Sci. Total
577 Environ., 593-594, 462-469, http://dio.org/10.1016/j.scitotenv.2017.03.088, 2017.
578 Du, Z., Hu, M., Peng, J., Zhang, W., Zheng, J., Gu, F., Qin, Y., Yang, Y., Li, M., Wu, Y., Shao, M., and
579 Shuai, S.: Comparison of primary aerosol emission and secondary aerosol formation from gasoline
580 direct injection and port fuel injection vehicles, Atmos. Chem. Phys., 18(12), 9011-9023,
581 http://dio.org/10.5194/acp-18-9011-2018, 2018.
582 Fu, H., Wang, Y., Li, X., and Shuai, S.: Impacts of cold-start and gasoline RON on particulate emission
583 from vehicles powered by GDI and PFI engines, SAE Technical Paper 2014-01-2836, http://dio.org/
584 10.4271/2014-01-2836, 2014.
585 Fushimi, A., Kondo, Y., Kobayashi, S., Fujitani, Y., Saitoh, K., Takami, A., and Tanabe, K.:
586 Chemical composition and source of fine and nanoparticles from recent direct injection
587 gasoline passenger cars: Effects of fuel and ambient temperature, Atmos Environ, 124, 77-84,
588 http://dio.org/10.1016/j.atmosenv.2015.11.017, 2016.
589 Giechaskiel, B., Maricq, M., Ntziachristos, L., Dardiotis, C., Wang, X., Axmann, H., Bergmann, A., and
590 Schindler, W.: Review of motor vehicle particulate emissions sampling and measurement: From
591 smoke and filter mass to particle number, J. Aerosol Sci., 67, 48-86,
592 http://dio.org/10.1016/j.jaerosci.2013.09.003, 2014.
593 Guo, S., Hu, M., Guo, Q., Zhang, X., Zheng, M., Zheng, J., Chang, C. C., Schauer, J. J., and Zhang, R.:
594 Primary sources and secondary formation of organic aerosols in Beijing, China, Environ. Sci.
595 Technol., 18(46), 9846 – 9853, 2012.
596 Hedge, M., Weber, P., Gingrich, J., Alger, T., and Khalek, I. A.: Effect of EGR on Particle Emissions
597 from a GDI Engine, SAE Int. J. Engines, 4(1), 650- 666, http://dio.org/10.4271/2011-01-0636, 2011.
598 Hou, C., Shao, L., Hu, W., Zhang, D., Zhao, C., Xing, J., Huang, X., and Hu, M.: Characteristics
599 and aging of traffic-derived particles in a highway tunnel at a coastal city in southern China,
600 Sci Total Environ, 619-620, 1385-1393, http://dio.org/10.1016/j.scitotenv.2017.11.165, 2018.
601 Hu, W., Niu, H., Zhang, D., Wu, Z., Chen, C., Wu, Y., Shang, D., and Hu, M.: Insights into a dust event
602 transported through Beijing in spring 2012: Morphology, chemical composition and impact on
603 surface aerosols, Sci. Total Environ., 565, 287-298, http://dio.org/10.1016/j.scitotenv.2016.04.175,
604 2016.
605 Huang, R., Zhang, Y., Bozzetti, C., Ho, K., Cao, J., Han, Y., Daellenbach, K. R., Slowik, J. G., Platt, S.
606 M., Canonaco, F., Zotter, P., Wolf, R., Pieber, S. M., Bruns, E. A., Crippa, M., Ciarelli, G.,
607 Piazzalunga, A., Schwikowski, M., Abbaszade, G., Schnelle-Kreis, J., Zimmermann, R., An, Z.,

608 Szidat, S., Baltensperger, U., Haddad, I. E., and Prévôt, A. S. H.: High secondary aerosol
609 contribution to particulate pollution during haze events in China, Nature, 514(7521), 218-222,
610 http://dio.org/10.1038/nature13774, 2014.
611 Hwa, M., and Yu, T.: Development of real-world driving cycles and estimation of emission factors
612 for in-use light-duty gasoline vehicles in urban areas, Environ Monit Assess, 186, 3985-3994,
613 http://dio.org/10.1007/s10661-014-3673-1, 2014.
614 Jacobson, M. Z.: Strong radiative heating due to the mixing state of black carbon in atmospheric aerosols,
615 Nature, 409(6821), 695-697, http://dio.org/10.1038/35055518, 2001.
616 Jang, M. S., Czoschke, N. M., Lee, S., and Kamens, R. M.: Heterogeneous atmospheric aerosol
617 production by acid-catalyzed particle-phase reactions, Science, 298(5594), 814-817,
618 http://dio.org/10.1126/science.1075798, 2002.
619 Jang, M., Czoschke, N. M., and Northcross, A. L.: Atmospheric organic aerosol production by
620 heterogeneous acid-catalyzed reactions, Chemphyschem, 5(11), 1647-1661,
621 http://dio.org/10.1002/cphc.200301077, 2004.
622 Jathar, S. H., Gordon, T. D., Hennigan, C. J., Pye, H. O. T., Pouliot, G., Adams, P. J., Donahue, N. M.,
623 and Robinson, A. L.: Unspeciated organic emissions from combustion sources and their influence
624 on the secondary organic aerosol budget in the United States, P. Natl. Acad. Sci. USA, 111(29),
625 10473-10478, http://dio.org/10.1073/pnas.1323740111, 2014.
626 Kanakidou, M., Seinfeld, J. H., Pandis, S. N., Barnes, I., Dentener, F. J., Facchini, M. C., Van Dingenen,
627 R., Ervens, B., Nenes, A., Nielsen, C. J., Swietlicki, E., Putaud, J. P., Balkanski, Y., Fuzzi, S., Horth,
628 J., Moortgat, G. K., Winterhalter, R., Myhre, C., Tsigaridis, K., Vignati, E., Stephanou, E. G., and
629 Wilson, J.: Organic aerosol and global climate modelling: A review, Atmos. Chem. Phys., 5, 1053-
630 1123, http://dio.org/10.5194/acp-5-1053-2005, 2005.
631 Khalek, I. A., Bougher, T., and Jetter, J. J.: Particle Emissions from a 2009 gasoline direct injection
632 engine using different commercially available fuels, SAE Int. J. Fuels Lubr., 3(2), 623- 637,
633 http://dio.org/10.4271/2010-01-2117, 2010.
634 Kuwata, M., Liu, Y., McKinney, K., and Martin, S.T.: Physical state and acidity of inorganic sulfate
635 can regulate the production of secondary organic material from isoprene photooxidation
636 products, Phys Chem Chem Phys: PCCP, 17, 5670-5678, http://dio.org/10.1039/C4CP04942J,
637 2015.
638 Lack, D.A., Langridge, J.M., Bahreini, R., Cappa, C.D., Middlebrook, A.M., and Schwarz, J.P.:
639 Brown carbon and internal mixing in biomass burning particles, P Natl Acad Sci USA, 109,
640 http://dio.org/14802-14807, 10.1073/pnas.1206575109, 2012.
641 Lambe, A.T., Ahern, A.T., Wright, J.P., Croasdale, D.R., Davidovits, P., and Onasch, T.B.:
642 Oxidative aging and cloud condensation nuclei activation of laboratory combustion soot, J
643 Aerosol Sci, 79, 31-39, http://dio.org/10.1016/j.jaerosci.2014.10.001, 2015.
644 Lang-Yona, N., Abo-Riziq, A., Erlick, C., Segre, E., Trainic, M., and Rudich, Y.: Interaction of
645 internally mixed aerosols with light, Phys Chem Chem Phys, 12, 21-31,
646 http://dio.org/10.1039/B913176K, 2010.
647 Laskin, A., Laskin, J., and Nizkorodov, S.A.: Chemistry of Atmospheric Brown Carbon, Chem Rev,
648 115, 4335-4382, http://dio.org/10.1021/cr5006167, 2015.
649 Li, W., and Shao, L.: Transmission electron m icroscopy study of aerosol particles from the brown hazes
650 in northern china, J. Geophys. Res.-Atmos., http://dio.org/D09302, 2009.
651 Liati, A., Schreiber, D., Dasilva, Y. A. R., and Eggenschwiler, P. D.: Ultrafine particle emissions from

modern gasoline and diesel vehicles: An electron microscopic perspective, Environ. Pollut., 239, 661-669, http://dio.org/10.1016/j.envpol.2018.04.081, 2018.

Liu, L., Kong, S., Zhang, Y., Wang, Y., Xu, L., Yan, Q., Lingaswamy, A. P., Shi, Z., Lv, S., Niu, H., Shao, L., Hu, M., Zhang, D., Chen, J., Zhang, X., and Li, W.: Morphology, composition, and mixing state of primary particles from combustion sources - crop residue, wood, and solid waste, Sci. Rep.-UK, http://dio.org/10.1038/s41598-017-05357-2, 2017.

Loh, N.D., Hampton, C.Y., Martin, A.V., Starodub, D., Sierra, R.G., Barty, A., Aquila, A., Schulz, J., Lomb, L., Steinbrener, J., Shoeman, R.L., Kassemeyer, S., Bostedt, C., Bozek, J., Epp, S.W., Erk, B., Hartmann, R., Rolles, D., Rudenko, A., Rudek, B., Foucar, L., Kimmel, N., Weidenspointner, G., Hauser, G., Holl, P., Pedersoli, E., Liang, M., Hunter, M.M., Gumprecht, L., Coppola, N., Wunderer, C., Graafsma, H., Maia, F.R.N.C., Ekeberg, T., Hantke, M., Fleckenstein, H., Hirsemann, H., Nass, K., White, T.A., Tobias, H.J., Farquar, G.R., Benner, W.H., Hau-Riege, S.P., Reich, C., Hartmann, A., Soltau, H., Marchesini, S., Bajt, S., Barthelmess, M., Bucksbaum, P., Hodgson, K.O., Strueder, L., Ullrich, J., Frank, M., Schlichting, I., Chapman, H.N., and Bogan, M.J.: Fractal morphology, imaging and mass spectrometry of single aerosol particles in flight, Nature, 486, 513-517, http://dio.org/10.1038/nature11222, 2012.

Lu, K.D., Hofzumahaus, A., Holland, F., Bohn, B., Brauers, T., Fuchs, H., Hu, M., Häseler, R., Kita, K., Kondo, Y., Li, X., Lou, S.R., Oebel, A., Shao, M., Zeng, L.M., Wahner, A., Zhu, T., Zhang, Y.H., and Rohrer, F.: Missing OH source in a suburban environment near Beijing: observed and modelled OH and HO_2 concentrations in summer 2006, Atmos Chem Phys, 13, 1057-1080, http://dio.org/10.5194/acp-13-1057-2013, 2013.

Luo, Y., Zhu, L., Fang, J., Zhuang, Z., Guan, C., Xia, C., Xie, X., and Huang, Z.: Size distribution, chemical composition and oxidation reactivity of particulate matter from gasoline direct injection (GDI) engine fueled with ethanol-gasoline fuel, Appl. Therm. Eng., 89, 647-655, http://dio.org/10.1016/j.applthermaleng.2015.06.060, 2015.

Ma, Q., Wu, Y., Zhang, D., Wang, X., Xia, Y., Liu, X., Tian, P., Han, Z., Xia, X., Wang, Y., and Zhang, R.: Roles of regional transport and heterogeneous reactions in the $PM_{2.5}$ increase during winter haze episodes in Beijing, Sci Total Environ, 599, 246-253, http://dio.org/10.1016/j.scitotenv.2017.04.193, 2017.

Maricq, M. M., Szente, J., Loos, M., and Vogt, R.: Motor vehicle PM emissions measurement at LEV III levels, SAE Int. J. Engines, 4(1), 597- 609, http://dio.org/10.4271/2011-01-0623, 2011.

Mauldin, R. L. I., Berndt, T., Sipilae, M., Paasonen, P., Petaja, T., Kim, S., Kurten, T., Stratmann, F., Kerminen, V., and Kulmala, M.: A new atmospherically relevant oxidant of sulphur dioxide, Nature, 488(7410), 193-196, http://dio.org/10.1038/nature11278, 2012.

National Bureau of Statistics of China, 2018. China Statistical Yearbook 2018, part sixteen: Transportation, post and telecommunications and software industry. Available on line at: http://www.stats.gov.cn/tjsj/ndsj/2018/indexch.htm, 2018.

Niu, H., Cheng, W., Hu, W., and Pian, W.: Characteristics of individual particles in a severe short-period haze episode induced by biomass burning in Beijing, Atmos. Pollut. Res., 7(6), 1072-1081, http://dio.org/10.1016/j.apr.2016.05.011, 2016.

Niu, H., Hu, W., Zhang, D., Wu, Z., and Guo, S.: Variations of fine particle physiochemical properties during a heavy haze episode in the winter of Beijing, Sci Total Environ, 571, 103-109, http://dio.org/10.1016/j.scitotenv.2016.07.147, 2016.

Niu, H., Shao, L., and Zhang, D.: Aged status of soot particles during the passage of a weak cyclone in Beijing, Atmos. Environ., 45(16), 2699-2703, http://dio.org/10.1016/j.atmosenv.2011.02.056, 2011.

Okada, K., Qin, Y., and Kai, K.: Elemental composition and mixing properties of atmospheric mineral particles collected in Hohhot, China, Atmos. Res., 73(1-2), 45-67, http://dio.org/10.1016/j.atmosres.2004.08.001, 2005.

Peng, J., Hu, M., Guo, S., Du, Z., Shang, D., Zheng, J., Zheng, J., Zeng, L., Shao, M., Wu, Y., Collins, D., and Zhang, R.: Ageing and hygroscopicity variation of black carbon particles in Beijing measured by a quasi-atmospheric aerosol evolution study (QUALITY) chamber, Atmos. Chem. Phys., 17(17), 10333-10348, http://dio.org/10.5194/acp-17-10333-2017, 2017.

Peng, J.F., Hu, M., Wang, Z.B., Huang, X.F., Kumar, P., Wu, Z.J., Guo, S., Yue, D.L., Shang, D.J., Zheng, Z., and He, L.Y.: Submicron aerosols at thirteen diversified sites in China: size distribution, new particle formation and corresponding contribution to cloud condensation nuclei production, Atmos Chem Phys, 14, 10249-10265, 10.5194/acp-14-10249-2014, 2014.

Petzold, A., Marsh, R., Johnson, M., Miller, M., Sevcenco, Y., Delhaye, D., Ibrahim, A., Williams, P., Bauer, H., Crayford, A., Bachalo, W. D., and Raper, D.: Evaluation of methods for measuring particulate matter emissions from gas turbines, Environ. Sci. Technol., 45(8), 3562-3568, 2011.

Rönkkö, T., Lähde, T., Heikkilä, J., Pirjola, L., Bauschke, U., Arnold, F., Schlager, H., Rothe, D., Yli-Ojanperä, J., and Keskinen, J.: Effects of gaseous sulphuric acid on diesel exhaust nanoparticle formation and characteristics, Environ. Sci. Technol., 47(20), 11882-11889, http://dio.org/10.1021/es402354y, 2013.

Scott, C. E., Rap, A., Spracklen, D. V., Forster, P. M., Carslaw, K. S., Mann, G. W., Pringle, K. J., Kivekas, N., Kulmala, M., Lihavainen, H., and Tunved, P.: The direct and indirect radiative effects of biogenic secondary organic aerosol, Atmos. Chem. Phys., 14(1), 447-470, http://dio.org/10.5194/acp-14-447-2014, 2014.

Shao, L., Hu, Y., Fan, J., Wang, J., Wang, J., and Ma, J.: Physicochemical characteristics of aerosol particles in the Tibetan Plateau: Insights from TEM-EDX analysis, J. Nanosci. Nanotechno., 17(9), 6899-6908, http://dio.org/10.1166/jnn.2017.14472, 2017.

Shao, L., Hu, Y., Shen, R., Schäfer, K., Wang, J., Wang, J., Schnelle-Kreis, J., Zimmermann, R., Bérubé, K., and Suppan, P.: Seasonal variation of particle-induced oxidative potential of airborne particulate matter in Beijing, Sci. Total Environ., 579, 1152-1160, http://dio.org/10.1016/j.scitotenv.2016.11.094, 2017.

Song, C., Na, K., Warren, B., Malloy, Q., and Cocker, D.R.: Secondary Organic Aerosol Formation from m-Xylene in the Absence of NOx, Environ Sci Technol, 41, 7409-7416, http://dio.org/10.1021/es070429r, 2007.

Song, M., Zhang, C., Wu, H., Mu, Y., Ma, Z., Zhang, Y., Liu, J., and Li, X.: The influence of OH concentration on SOA formation from isoprene photooxidation, Sci Total Environ, 650, 951-957, http://dio.org/10.1016/j.scitotenv.2018.09.084, 2019.

Shi, Z., Vu, T., Kotthaus, S., Harrison, R. M., Grimmond, S., Yue, S., Zhu, T., Lee, J., Han, Y., Demuzere, M., Dunmore, R. E., Ren, L., Liu, D., Wang, Y., Wild, O., Allan, J., Acton, W. J., Barlow, J., Barratt, B., Beddows, D., Bloss, W. J., Calzolai, G., Carruthers, D., Carslaw, D. C., Chan, Q., Chatzidiakou, L., Chen, Y., Crilley, L., Coe, H., Dai, T., Doherty, R., Duan, F., Fu, P., Ge, B., Ge, M., Guan, D., Hamilton, J. F., He, K., Heal, M., Heard, D., Hewitt, C. N., Hollaway, M., Hu, M., Ji, D., Jiang, X., Jones, R., Kalberer, M., Kelly, F. J., Kramer, L., Langford, B., Lin, C., Lewis, A. C., Li, J., Li, W., Liu, H., Liu, J., Loh, M., Lu, K., Lucarelli, F., Mann, G., McFiggans, G., Miller, M. R., Mills, G.,

Monk, P., Nemitz, E., O'Connor, F., Ouyang, B., Palmer, P. I., Percival, C., Popoola, O., Reeves, C., Rickard, A. R., Shao, L., Shi, G., Spracklen, D., Stevenson, D., Sun, Y., Sun, Z., Tao, S., Tong, S., Wang, Q., Wang, W., Wang, X., Wang, X., Wang, Z., Wei, L., Whalley, L., Wu, X., Wu, Z., Xie, P., Yang, F., Zhang, Q., Zhang, Y., Zhang, Y., and Zheng, M.: Introduction to the special issue "In-depth study of air pollution sources and processes within Beijing and its surrounding region (APHH-Beijing)", Atmos. Chem. Phys., 19(11), 7519-7546, http://dio.org/10.5194/acp-19-7519-2019, 2019.

Suarez-Bertoa, R., Zardini, A. A., Platt, S. M., Hellebust, S., Pieber, S. M., El Haddad, I., Temime-Roussel, B., Baltensperger, U., Marchand, N., Prévôt, A. S. H., and Astorga, C.: Primary emissions and secondary organic aerosol formation from the exhaust of a flex-fuel (ethanol) vehicle, Atmos. Environ., 117, 200-211, http://dio.org/10.1016/j.atmosenv.2015.07.006, 2015.

Szybist, J. P., Youngquist, A. D., Barone, T. L., Storey, J. M., and Moore, W. R.: Ethanol blends and engine operating strategy effects on light-duty spark-ignition engine particle emissions, Energ. Fuel., 25(11), 4977-4985, http://dio.org/10.1021/ef201127y, 2011.

Wang, W., Shao, L., Li, J., Chang, L., Zhang, D., Zhang, C., and Jiang, J.: Characteristics of individual particles emitted from an experimental burning chamber with coal from the lung cancer area of Xuanwei, China, Aerosol Air Qual. Res., 19(2), 355-363, http://dio.org/10.4209/aaqr.2018.05.0187, 2019.

Xing, J., Shao, L., Zhang, W., Peng, J., Wang, W., Hou, C., Shuai, S., Hu, M., and Zhang, D.: Morphology and composition of particles emitted from a port fuel injection gasoline vehicle under real-world driving test cycles, J. Environ. Sci-China, 76, 339-348, http://dio.org/10.1016/j.jes.2018.05.026, 2019.

Xing, J., Shao, L., Zheng, R., Peng, J., Wang, W., Guo, Q., Wang, Y., Qin, Y., Shuai, S., and Hu, M.: Individual particles emitted from gasoline engines: Impact of engine types, engine loads and fuel components, J. Clean. Prod., 149, 461-471, http://dio.org/10.1016/j.jclepro.2017.02.056, 2017.

Yu, L., Wang, G., Zhang, R., Zhang, L., Song, Y., Wu, B., Li, X., An, K., and Chu, J.: Characterization and source apportionment of $PM_{2.5}$ in an urban environment in Beijing, Aerosol Air Qual. Res., 13(2), 574-583, 2013.

Zhang, H., Cheng, S., Li, J., Yao, S., and Wang, X.: Investigating the aerosol mass and chemical components characteristics and feedback effects on the meteorological factors in the Beijing-Tianjin-Hebei region, China, Environ. Pollut., 244, 495-502, http://dio.org/10.1016/j.envpol.2018.10.087, 2019.

Zhang, M., Li, Z., Xu, M., Yue, J., Cai, Z., Yung, K.K.L., and Li, R.: Pollution characteristics, source apportionment and health risks assessment of fine particulate matter during a typical winter and summer time period in urban Taiyuan, China, Hum Ecol Risk Assess, http://dio.org/10.1080/10807039.2019.1684184, 2019.

Zhang, Y., Yuan, Q., Huang, D., Kong, S., Zhang, J., Wang, X., Lu, C., Shi, Z., Zhang, X., Sun, Y., Wang, Z., Shao, L., Zhu, J., and Li, W.: Direct observations of fine primary particles from residential coal burning: Insights into their morphology, composition, and hygroscopicity, J. Geophys. Res.-Atmos., 123(22), 12,964-12,979, http://dio.org/10.1029/2018JD028988, 2018.

Zhu, J., Penner, J. E., Lin, G., Zhou, C., Xu, L., and Zhuang, B.: Mechanism of SOA formation determines magnitude of radiative effects, P. Natl. Acad. Sci. USA, 114(48), 12685-12690, http://dio.org/10.1073/pnas.1712273114, 2017.

Zimmerman, N., Wang, J. M., Jeong, C., Ramos, M., Hilker, N., Healy, R. M., Sabaliauskas, K., Wallace,

784 J. S., and Evans, G. J.: Field measurements of gasoline direct injection emission factors: Spatial and
785 seasonal variability, Environ. Sci. Technol., 50(4), 2035-2043,
786 http://dio.org/10.1021/acs.est.5b04444, 2016.

787

List of tables:

Table 1 Comparison of chemical components between various sources including fossil fuels, biomass burning and urban waste burning

Study	Source	Particle of type and relative percentages	Chemical composition of organic particles
This study	GDI-engine vehicles	Organic particles (OM) (32%), Soot (32%), Ca-rich particles (26%), S-rich (5%) and metal-containing particles (4%)	OM with Ca and weak P, S, and Zn
Xing et al. (2019)	PFI-engine vehicles	OM (44%), soot (23%), Ca-rich particles (20%), S-rich (6%) and metal-containing particles (6%).	OM with Ca and weak P, S, and Zn.
Liati et al. (2018)	GDI, PFI and diesel vehicles	Soot, OM (called ash-bearing soot particles) and ash particles.	OM with Ca, S, P, Fe and minor Zn.
Liu et al. (2017)	Crop residue combustion	OM (27%), OM-K (43%), OM-soot-K (27%), soot-OM (3%).	OM particles with K content.
Liu et al. (2017)	Wood combustion	OM (16%), soot (18%), OM-K (22%), OM-soot-K (15%), soot-OM (29%).	OM particles with K content.
Wang et al. (2019)	Coal burning	OM (38%), soot (40%), S-rich particles (2%), and mineral particles (18%).	OM mainly consisted of C, O and Si.
Zhang et al. (2018)	Residential coal burning	OM (51%), OM-S (24%), soot-OM (23%), S-rich (1%), metal-rich particles (1%), mineral particles (1%).	OM contained C, O, and Si with minor amounts of S and Cl.

List of figures:

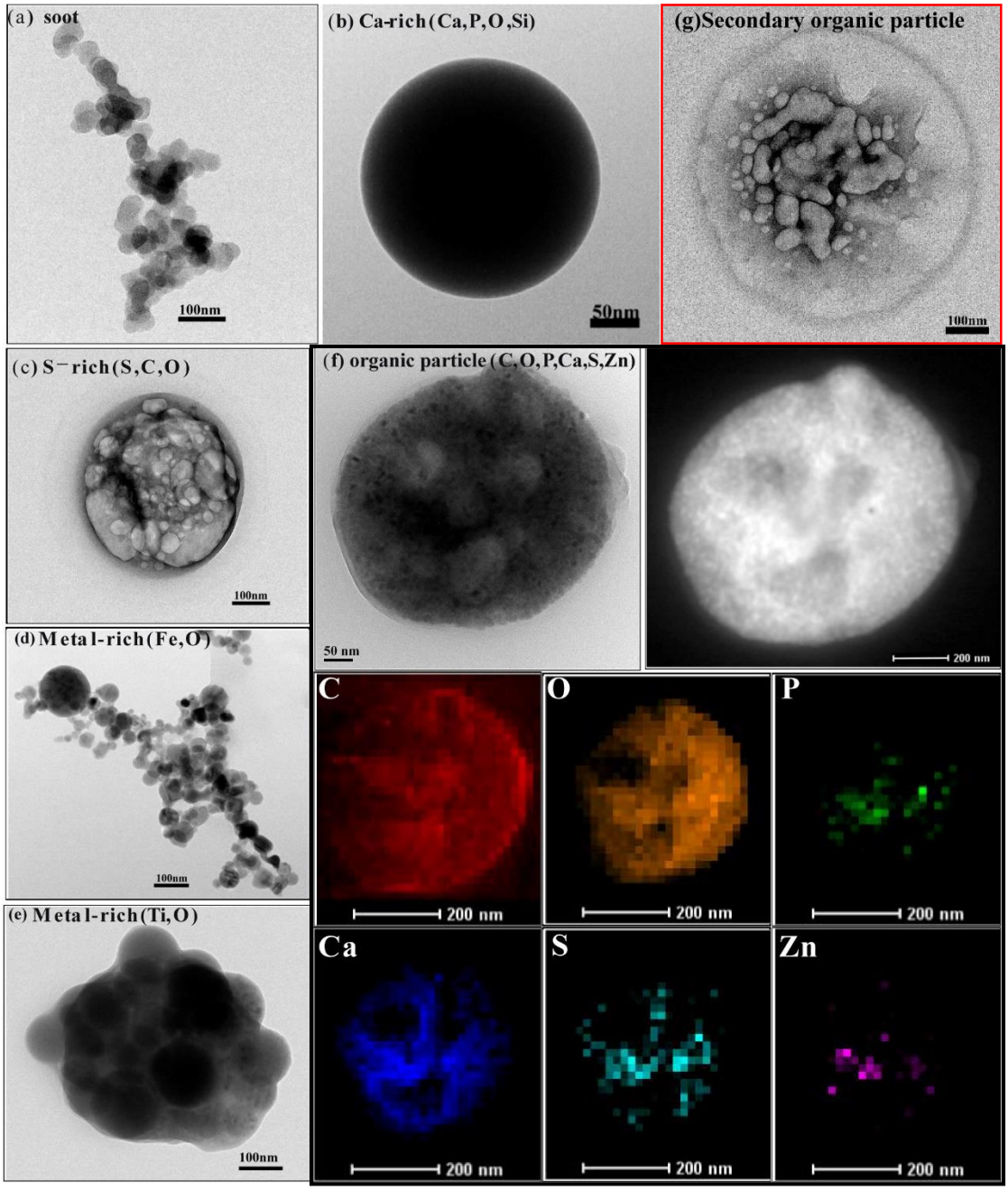

Figure 1. TEM images of the individual primary particles emitted from the GDI-engine gasoline vehicle and the secondary organic particle in the chamber after exposure to ambient sunlight for 3.5 hours. (a) soot particle; (b) Ca-rich particle; (c) S-rich particles; (d) Metal-rich particles (Fe); (e) Metal-rich particles (Ti); (f) bright-field-TEM and dark-field-TEM image of organic particles, and others are the mapping of the C, O, P, Ca, S, and Zn in the organic particle; (g) secondary organic particle in chamber.

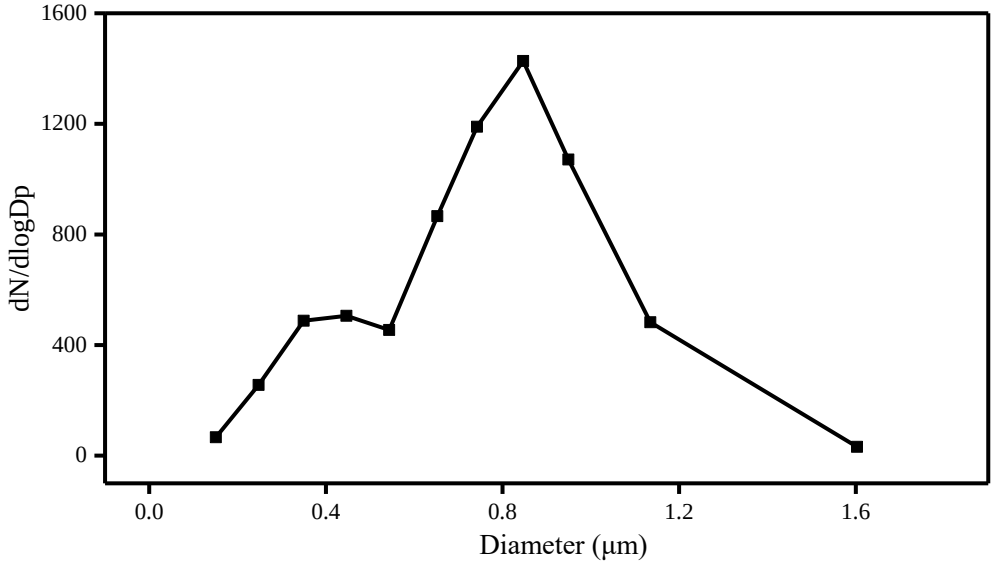

802

803 Figure 2. Size distribution of analyzed particles emitted from the GDI-engine gasoline
804 vehicles by the TEM images. In total, 2880 particles were analyzed from the GDI-
805 engine vehicles. Particles smaller than 0.25 μm should have been underestimated
806 because of the collection efficiency of the impactor.

807

808

(a)

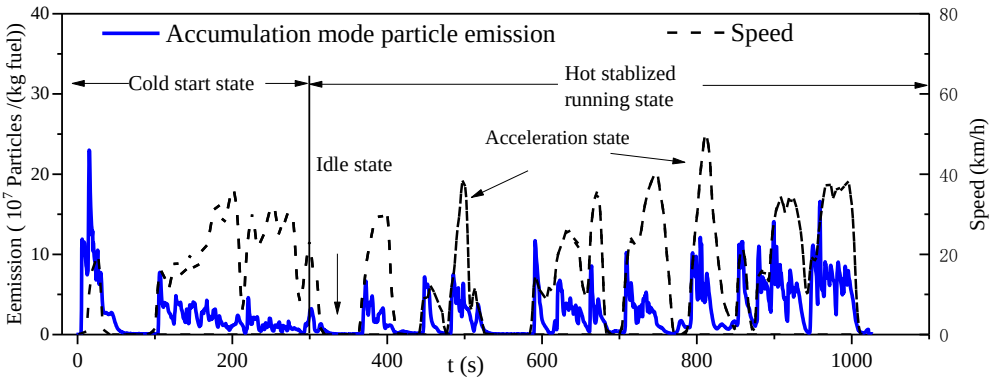

(b)

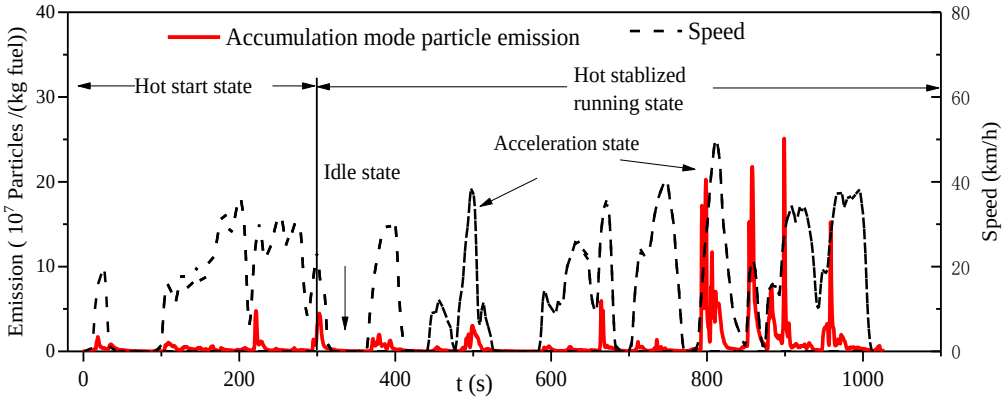

Figure 3. Particles in accumulation mode from the GDI vehicle during cold start (a) and hot start (b) driving cycle. The vehicle speed is also shown for reference. Before the test with cold start, the temperatures of the engine coolant and oil could not differ by more than 2 °C during the soak temperature. The hot start test was conducted within 5 mins after the cold start test. The number concentration of particles during the tests was monitored by DMS 500.

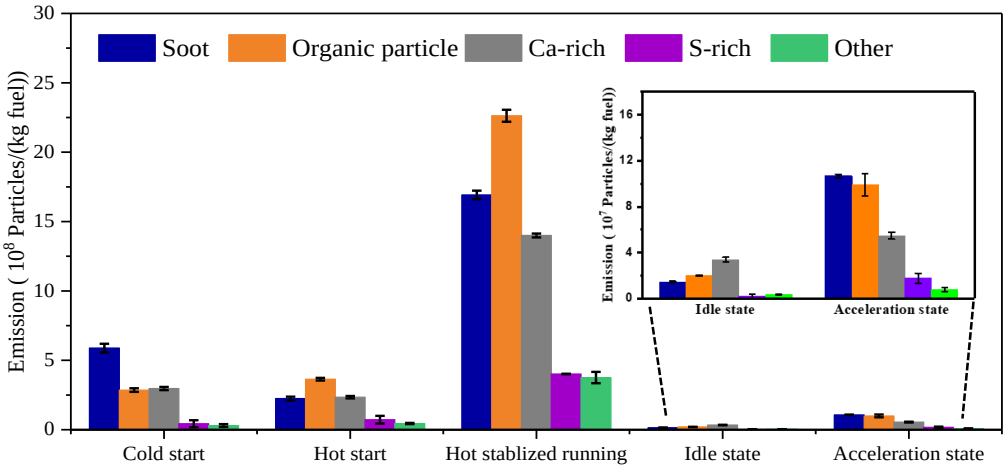

Figure 4. The number of different type particles in the emissions from the GDI vehicle under the different running states by the burning of per unit of fuel, including cold start, hot start, hot stabilization, idle, and acceleration states. Data presented as mean ± standard deviation, N = 3.

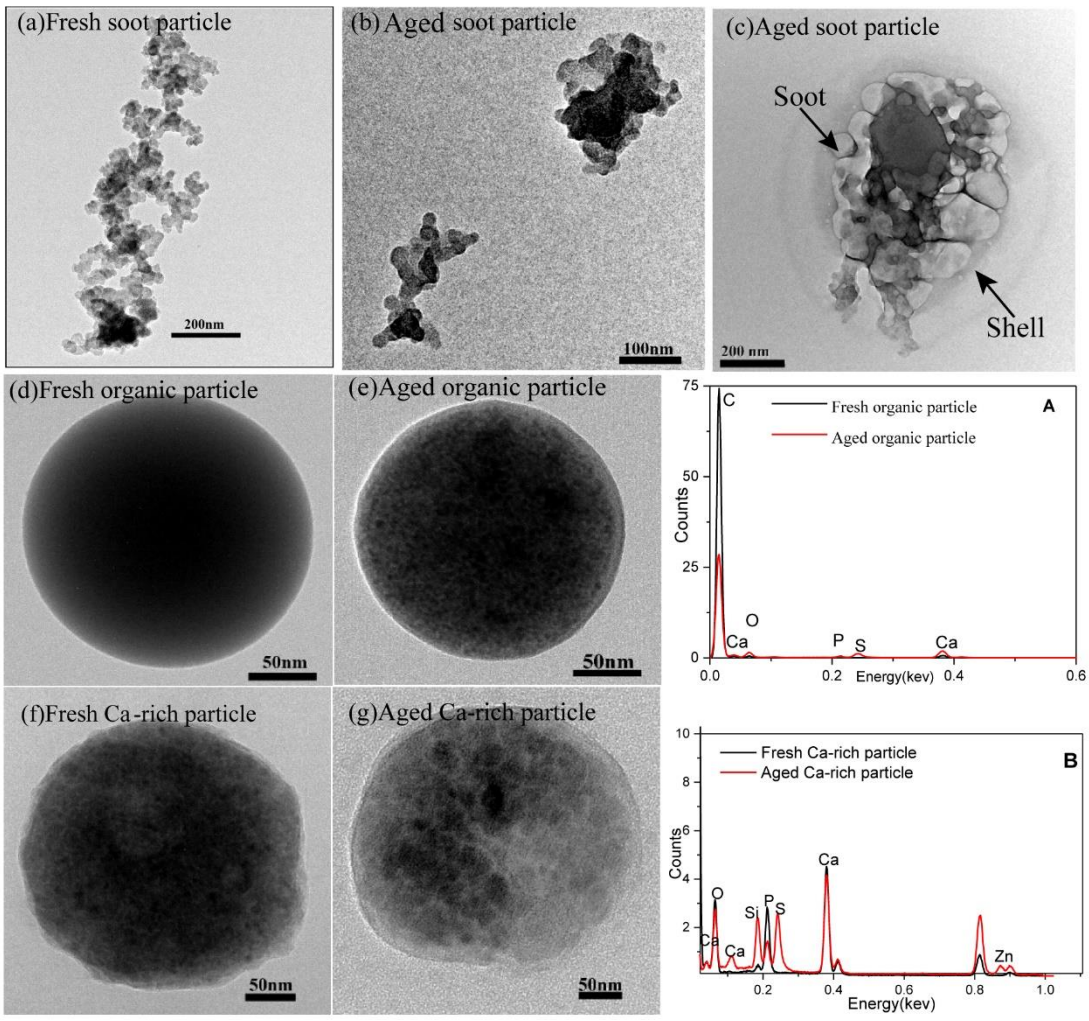

Figure 5. TEM images of particles in the chamber after exposure to ambient sunlight for 3.5 hours. (a) Fresh soot particles; (b) Aged soot particles; (c) Aged soot particle (d) Fresh organic particle (e) Aged organic particle (f) Fresh Ca-rich particle (g) Aged Ca-rich particle (A) EDX spectrum for a fresh organic particle and an aged organic particle. (B) EDX spectrum for a fresh organic particle and an aged Ca-rich particle.